# Structure, dielectric and impedance properties of $BaTiO_3$–$Bi(Y_{0.5}Yb_{0.5})O_3$ lead-free ceramics

Xuechen Huang · Hanxing Liu · Hua Hao ·
Zhijian Wang · Wei Hu · Qi Xu · Lin Zhang ·
Minghe Cao

**Abstract** $(1 - x)BaTiO_3$–$xBi(Y_{0.5}Yb_{0.5})O_3$ (BT–BYYb, x = 0.01–0.12) ceramics were prepared via solid-state processing techniques. The structure, dielectric and impedance properties of $(1 - x)$BT–xBYYb ceramics are studied. The studies show that the ceramics are in tetragonal phase when x ≤ 0.07, transform to pseudocubic phase at x ≥ 0.08. The grain growth is obviously suppressed for $(1 - x)$BT–xBYYb samples with x value. Dielectric properties are depressed and dielectric peaks are broadened with x. $T_m$ first increases and then decreases. BT–BYYb system exhibits diffused phase transition and good temperature stability, which is due to the increased cation disorder, forming the local difference of the polar region due to the size and charge difference and inducing many different regions with different Curie points. The samples can meet the temperature requirements of X8R characteristics at 1 kHz with: ε ∼ 1330, tanδ ∼ 0.0076, $|\triangle C/C| \le \pm 15$ % (−55 to 150 °C) for x = 0.11 and ε ∼ 1032, tanδ ∼ 0.012, $|\triangle C/C| \le \pm 15$ % (−55 to 170 °C) for x = 0.12, respectively. The activation energy of the bulk material obtained from conduction and relaxation first increases and then decreases with increasing BYYb concentration. The different activation energy indicates various mechanisms are involved in the conduction and relaxation process, which may be due to the mixed conduction or doubly ionized oxygen and thermal motions of titanium ions ($Ti^{4+}$) or doubly ionized oxygen, respectively.

## 1 Introduction

The multilayer ceramic capacitor (MLCC), characterized by its high capacitance and compactness, is the most widely used in electronic devices. It is reported [1] that trillions of pieces of MLCC are manufactured each year. Thus it has important significance in the investigation and development of the steady and high-performance dielectric materials that can satisfy the Electronic Industries Association (EIA) XR ($\triangle C/C_{25°C} = \pm 15$ % or less) characteristics. The dielectric material with the "core–shell" microstructure composed of chemically inhomogeneous grain is considered as a key factor to satisfy XR characteristics [2, 3]. $BaTiO_3$ based ceramics are modified by the doping species such as $BaNb_2O_6$ [4], $CaZrO_3$ [5], and oxides [6–8] to obtain a core–shell structure, which can satisfy the requirements of X8R characteristics ($\triangle C/C_{25°C} = \pm 15$ % or less, −55 to 150 °C). But there are few report that systems without "core–shell" structure or two dielectric peaks can satisfy the requirement of the XR temperature range [9].

The improvement of the degree of dispersion of ceramics is a good way to meet the requirement of XR characteristics of the dielectric ceramics as much as possible. Research on bismuth-based compounds gained popularity due to bismuth's similarities to lead. $BaTiO_3$–$BiMeO_3$ ($Sc^{3+}$ [10–12], $Yb^{3+}$ [13], $(Mg_{1/2}Ti_{1/2})^{3+}$ [14, 15], $Fe^{3+}$ [16–18], $Al^{3+}$ [19, 20], $(Zn_{1/2}Ti_{1/2})^{3+}$ [21, 22], $(Ni_{1/2}Ti_{1/2})^{3+}$ [23], $Y^{3+}$ [24]) solid solutions have been investigated by many researchers. When Bi is substituted for Ba in $BaTiO_3$, a material with a high dielectric constant and

X. Huang · H. Liu (✉) · H. Hao · Z. Wang · W. Hu · Q. Xu ·
L. Zhang · M. Cao
State Key Laboratory of Advanced Technology for Materials
Synthesis and Processing, School of Material Science and
Engineering, Wuhan University of Technology, Wuhan 430070,
People's Republic of China
e-mail: lhxhp@whut.edu.cn

minimal temperature dependence is achieved. This is due to a lowering of both the Curie temperature and the maximum permittivity [12]. The presence of lone-pair electrons from $Bi^{3+}$ in the $BaTiO_3$–$BiMeO_3$ system are believed to induce the strong bending or antisymmetric stretching of the B–O bonds, showing micro-region of compositional fluctuations [24]. $(1 - x)BaTiO_3$–$xBi(Zn_{1/2}Ti_{1/2})O_3$ systems also demonstrates stable dielectric properties over a wide temperature range at $x \geq 0.2$ in the pseudocubic phase [21, 22]. Both $BaTiO_3$–$BiYO_3$ [24] and $BaTiO_3$–$BiYbO_3$ [13] systems exhibit relaxor behavior and low temperature coefficient of dielectric constant. In addition, the diffuse phase transition of dual rare earth doped barium titanate ceramics is obviously much stronger than mono rare earth doped barium titanate ceramics, which is strongly dependent on the site preference of rare-earth impurity in $BaTiO_3$ sublattices [25, 26].

In this paper, a new lead-free $(1 - x)BT$–$xBYYb$ solid solution was selected to investigate the effects caused by the addition of BYYb to BT on structural, dielectric properties and impedance properties. $(1 - x)BT$–$xBYYb$ that exhibits a high degree of stability, obviously superior to $BaTiO_3$–$BiYO_3$ [24] and $BaTiO_3$–$BiYbO_3$ [13] in terms of stability in relative permittivity and operating temperature range. The mechanism of relaxation process and the conduction process are analyzed in detail.

## 2 Experimental

$(1 - x)BT$–$xBYYb$ powders were synthesized by solid state reactions. Reagent-grade barium titanate ($BaTiO_3$, Guangdong Fenghua Advanced Technology Holding Co. Ltd., >99.0 %), bismuth oxide ($Bi_2O_3$, Sinopharm Chemical Reagent Co. Ltd., >99.9 %), yttrium oxide ($Y_2O_3$, Aladdin Chemistry Co. Ltd., >99.9 %), ytterbium oxide ($Yb_2O_3$, Aladdin Chemistry Co. Ltd., >99.9 %) were weighted according to the nominal compositions and mixed for 24 h by ball milling in alcohol. After drying, the milled powders were calcined in air at 950 °C for 2 h, and then remilled in isopropyl alcohol for 24 h. To improve the green strength of the powder compacts, polyvinyl alcohol (PVA) binder was added to the powder and granulated. These green bodies were pressed into disks with 12 mm in diameter and 1.5 mm in thickness by uniaxial pressing at about 200 MPa, and then binder burned out at 650 °C, followed by sintering at 1250–1350 °C for 3 h in air.

Phase purity and structure of the ceramic powders were determined by X-ray powder diffraction (Cu Kα, k = 1.54056 Å, PANalytical X'Pert PRO, Eindhoven, Netherlands) operated at 40 kV and 40 mV, the lattice parameters were calculated by X'Pert HighScore Plus diffraction software. For dielectric measurement, the sintered ceramics were polished to obtain smooth and parallel surfaces. Then a silver paste was painted and fired at 800 °C for 30 min to form the electrode. Temperature dependence of dielectric properties and complex impedance were measured using an LCR meter (LCR, E4980A, Agilent, USA) connected to a computer controlled furnace. Complex impedance was measured over frequencies from 20 Hz to 2 MHz in a temperature range of 24–480 °C. The evaluation of each R (Resistance) component value for an assumed equivalent circuit was determined by the software Z-view.

## 3 Results and discussion

The XRD patterns of $(1 - x)BT$–$xBYYb$ ceramics sintered at 1250–1350 °C for 3 h are shown in Fig. 1a. It is observed that the stable perovskite phases are formed in samples with $x \leq 0.14$. When $x > 0.14$, the second phases can be seen, Fig. 1b shows the XRD diffraction patterns of $(1 - x)BT$–$xBYYb$ ($x = 0.01$–$0.12$) ceramics sintered at 1250–1350 °C for 3 h. It is clearly indicated that the crystal phase changes gradually from the tetragonal phase to the pseudocubic phase in the samples with $0.07 < x < 0.08$ from the splitting of (200) and (002) peak to (200) peaks as shown in Fig. 1c. Hence, the stable tetragonal phases can only be formed when $x \leq 0.07$ in the $(1 - x)BT$–$xBYYb$ system.

To obtain the precise lattice parameters of $(1 - x)BT$–$xBYYb$ ($x = 0$–$0.12$) samples, The lattice parameters calculated from the XRD data using Si standard sample of $(1 - x)BT$–$xBYYb$ ($x = 0$–$0.12$) [14], as shown in Fig. 2. It can be seen that the lattice parameters (a) increases monotonously and c first increases and then decreases with x for $(1 - x)BT$–$xBYYb$ with $x \leq 0.07$, these compositions stabilized in the tetragonal symmetry. The lattice parameters (a = c) continue to increase until $x \leq 0.11$, and then stay the same at $x = 0.12$, which implied that BYYb have no longer entered the unit-cell maintaining the perovskite structure of the solid solution. That is, the solubility limit for $(1 - x)BT$–$xBYYb$ perovskite structure is determined to be about $x = 0.11$. In addition, the tetragonal ratio c/a first increases and then decreases eventually equals to 1.

Figure 3 shows the SEM micrographs of the surfaces of $(1 - x)BT$–$xBYYb$ ceramics at 1350 °C for 3 h. All the ceramics are well sintered and process a dense microstructure. The grain growth is suppressed for $(1 - x)BT$–$xBYYb$ samples with x value. The normal grains and the strip-shaped grains are obviously observed in 0.88BT–0.12BYYb ceramic in Fig. 3i. In order to confirm the ingredient of the grains, energy-dispersive spectroscopy (EDS) analysis is employed. The EDS data of spots A (marked A) in Fig. 3g and spots B (marked B) in Fig. 3i
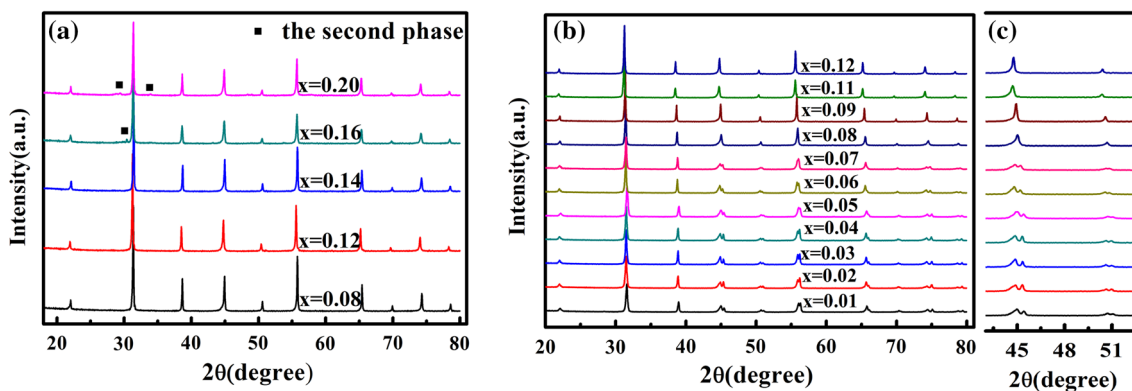
Fig. 1 X-ray diffraction patterns of $(1 - x)$BT–xBYYb ceramics sintered at 1300–1430 °C for 3 h. **a** 8 mol% $\leq x \leq$ 20 mol%, **b** 1 mol% $\leq x \leq$ 12 mol% and **c** enlarged from 43° to 52.5°
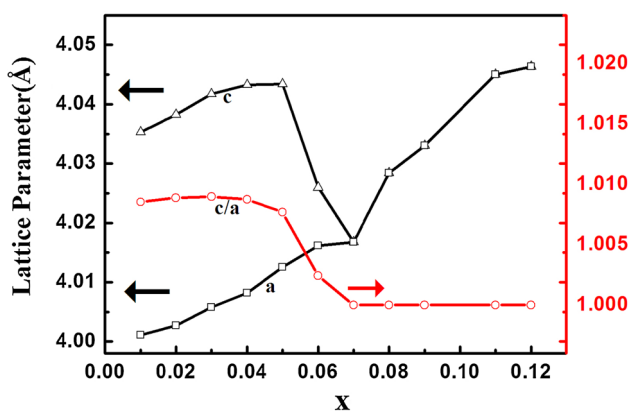


Fig. 2 Lattice parameters as a function of x

are shown in Table 1. EDS results of spots A show that $Yb^{3+}$ ions have a higher amount of substitution for Ti-site than $Y^{3+}$ ions, due to the closer ionic radius between $Ti^{4+}$ ions and $Yb^{3+}$ ions. However, $Yb^{3+}$ ions have the equivalent addition of $Y^{3+}$ ions. Excess $Y^{3+}$ ions locate at grain boundaries and inhibit grain growth. The EDS analysis of spots B reveals that the strip-shaped secondary grains are confirmed as Y-rich phases, which tend to segregate at grain boundaries and also inhibit grain growth. The secondary phases are confirmed by the XRD patterns using Si standard sample of 0.88BT–0.12BYYb.

Figure 4 shows the temperature dependence of the dielectric properties for $(1 - x)$BT–xBYYb (x = 0.01–0.12) ceramics at 1 kHz. The maximum value of the dielectric constant decreases with increasing BYYb content and it exhibits a broad maximum value of the dielectric permittivity, which may be attributed to the increased cation disorder due to the Ti-site and Ba-site substitution by $Y^{3+}$ or/ and $Yb^{3+}$ and $Bi^{3+}$, disrupting the long-range dipolar interaction and forming the local difference of the polar region due to the size and charge difference [24]. Figure 5 shows the temperature variation of capacitance of $(1 - x)$BT–xBYYb

(x = 0.11; 0.12) ceramics at 1 kHz. The best performance components are 0.89BT–0.11BYYb and 0.88BT–0.12BYYb, which meet the X8R requirements respectively at 1 kHz with: $\varepsilon \sim 1330$, $\tan\delta \sim 0.0076$, $|\triangle C/C| \leq \pm 15$ % ($-55$ to 150 °C) and $\varepsilon \sim 1032$, $\tan\delta \sim 0.012$, $|\triangle C/ C| \leq \pm 15$ % ($-55$ to 170 °C).

Figure 6 shows the maximum dielectric constant ($\varepsilon_m$) and the temperature at which the relative permittivity is maximum ($T_m$) as a function of composition for $(1 - x)$ BT–xBYYb (x = 0.01–0.12) at 100 kHz. The dielectric constant at $T_m$ decreases with increasing BYYb content. $T_m$ exhibits a slow decline with x at the compositions with x $\leq$ 0.04 in the tetragonal phase. Upon further increase in BYYb content, $T_m$ decreases rapidly, processing in the pseudocubic phase, which is a ferroelectric to paraelectric phase transition temperature. $T_m$ increases when x = 0.12, the second phases with the high Curie temperature may be responsible for the increase of $T_m$ and induce the deterioration of the dielectric properties [14].

In order to characterize the dielectric dispersion and diffuseness of BT–BYYb samples, Uchino and Nomura [27] modified the Curie–Weiss law for the diffuseness phase transition and given as

$$\frac{1}{\varepsilon} - \frac{1}{\varepsilon_m} = \frac{(T - T_m)^{\gamma}}{C} \tag{1}$$

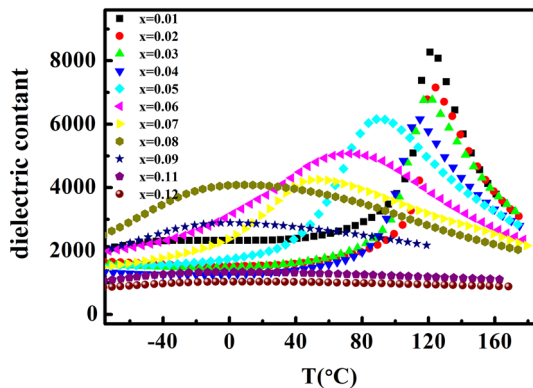where $\gamma$ and C are modified constants, with $1 < \gamma < 2$. The value of the parameter $\gamma$ gives information about the character of the phase transition. Its limiting values are $\gamma = 1$ and $\gamma = 2$. The value of $\gamma$ is 1 for the case of a normal ferroelectric and $\gamma = 2$ is valid for an ideal ferroelectric relaxor. The exponent $\gamma$ is obtained from the slope of $\log(1/\varepsilon - 1/\varepsilon_m)$ and $\log(T - T_m)$ plot, as shown in Fig. 7, which exhibits a good linear relation for BT–BYYb samples and $\gamma$ is between 1 and 2, Thus, BT–BYYb samples (x $\geq$ 0.05) are considered as relaxor ferroelectrics.
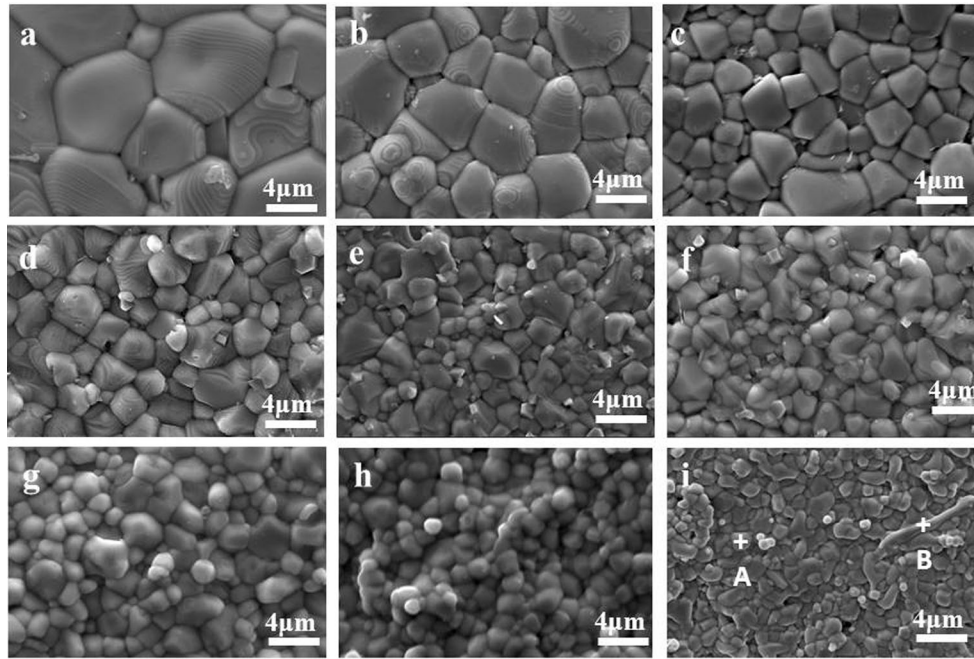
**Fig. 3** SEM micrographs of $(1 - x)$BT–BYYb (**a** x = 0.01, **b** x = 0.02, **c** x = 0.03, **d** = 0.04, **e** x = 0.05, **f** x = 0.06, **g** x = 0.08, **h** x = 0.11, **i** x = 0.12) ceramics sintered at 1350 °C for 3 h

**Table 1** The EDS data of the spots A and B shown in Fig. 3

| Spots | Atom (%) | | | | | |
|-------|------|------|-------|------|-------|-------|
| | Ba | Bi | Y | Yb | Ti | O |
| A | 16.56 | 1.26 | 1.67 | 2.31 | 11.58 | 66.62 |
| B | 11.07 | 1.05 | 16.16 | 3.7 | 11.2 | 56.83 |



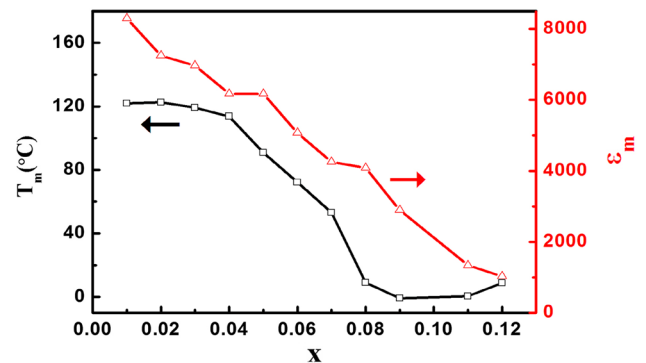**Fig. 5** Capacitance variation of $(1 - x)$BT–BYYb (x = 0.11; 0.12) samples as a function of temperature at 1 kHz



**Fig. 4** Dielectric constant as a function of temperature at 1 kHz for $(1 - x)$BT–BYYb (x = 0.01–0.12) ceramics
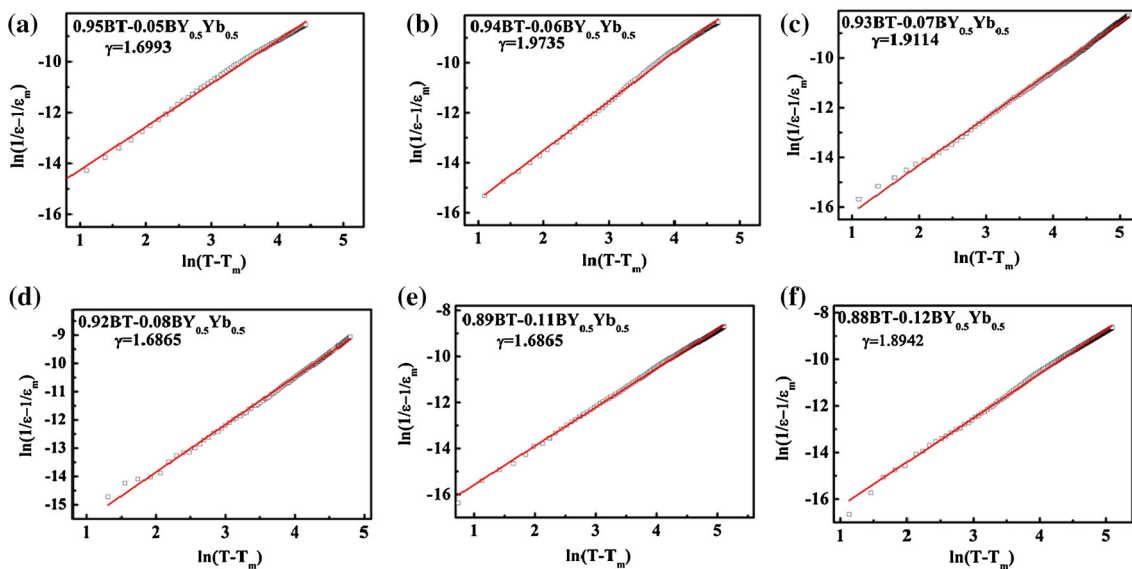
Impedance spectroscopy is a clear and nondestructive technique to carry out more detail analyses of dielectric properties and conduction mechanism in the materials [28].
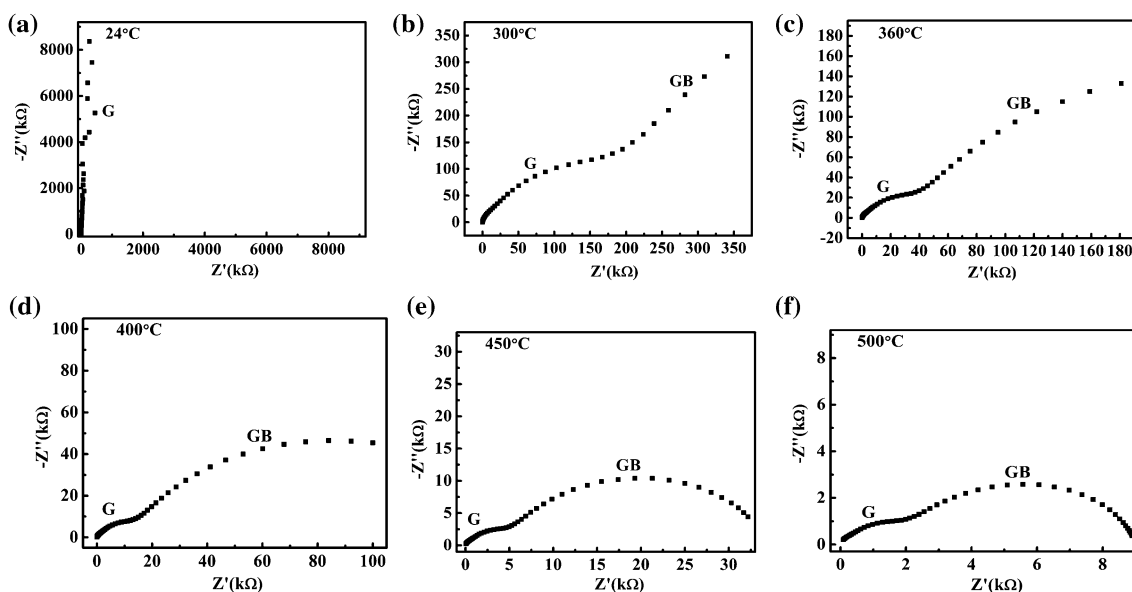


**Fig. 6** $T_m$ and $\varepsilon_m$ as a function of composition for BYYb at 100 kHz

**Fig. 7** Plots of $\ln(1/\varepsilon - 1/\varepsilon_m)$ versus $\ln(T - T_m)$ of $(1 - x)BT$–BYYb ceramics at 100 kHz. **a** x = 0.05, **b** x = 0.06, **c** x = 0.07, **d** x = 0.08, **e** x = 0.11, **f** x = 0.12



**Fig. 8** $(-Z'') - Z'$ plots and assignments of 0.98BT–0.02BYYb at different temperature. *G* grain, *GB* grain boundary

Figure 8a–f shows the variation of $(-Z'')$ with $Z'$ over a wide range of frequency (20 Hz–2 MHz) at different temperatures for 0.98BT–0.02BYYb ceramics. Above 300 °C, the impedance spectra consist of two "semi-circles" with a small semicircle arc at high frequencies and a large are at low frequencies. With the temperature increasing, the high-frequency arc becomes smaller and smaller, whereas the low-frequency arc tends to be a well-developed semicircle. The trend indicates the enhancement of grain resistance ($R_g$), grain boundary resistance ($R_{gb}$), The high-frequency arc is ascribed to be the dielectric response from the grain interiors (G) and the low-frequency are can be ascribed to be the dielectric response from the grain boundary (GB) as labeled in the figures, which is consistent with the brick-layer model for a polycrystalline material [29].

Figure 9 shows the plots of imaginary part of impedance $(-Z'')$ versus frequency for 0.98BT–0.02BYYb at different temperatures. Two distinct peaks at low and high frequencies are observed. The distinct peaks are not clearly visible for temperatures of 400–480 °C due to large difference in peak intensities. The peak values $(-Z''_{max})$
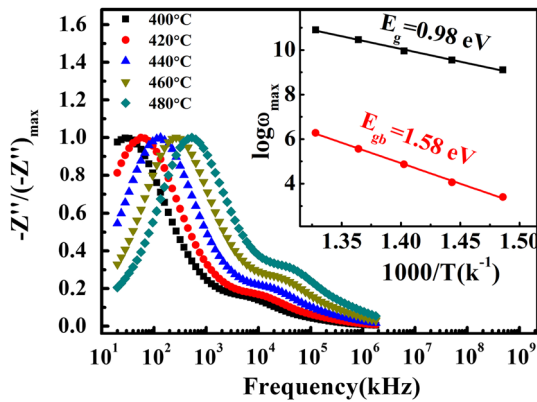
**Fig. 9** Variation of (a) imaginary part of impedance (Z″) with frequency for 0.98BT–0.02BYYb at high temperatures ranges from 400 to 480 °C. Inset shows temperature dependence of relaxation frequency



**Fig. 10** Arrhenius dependence for the relaxation time for (1 − x) BT–xBYYb (x = 0.02; 0.04; 0.06; 0.08; 0.11) at low frequency peak

decreases and the peak positions shift to higher frequency upon heating, indicating the decrease of the resistances of the grain and grain boundary as well as the decrease of the relaxation time, respectively. The space charge polarization is active at low frequencies and high temperatures. The merging of imaginary part with increasing frequency may be attributes to the decrease of space charge polarization in grain interiors [30]. Peak broadening with increasing temperature verifies the presence of temperature dependence relaxation phenomenon. The relaxation times τ were calculated from the frequencies at which the Z″$_{max}$ is observed. It exhibits a peak in a slightly asymmetric degree at each temperature. The relaxation is obtained by the formula $\tau_{max} = 1/\varpi_{max}$, The most probable relaxation time follows the Arrhenius law,

$$\omega_{max} = \omega_0 \exp\left(\frac{-E_a}{K_B T}\right) \qquad (2)$$

where $\omega_0$ is the pre-exponential factor. $E_a$ is the activation energy of relaxation process. In Fig. 9, the inset shows the activation energy ($E_a$) calculated from the least-squares fit to the points and found to be 1.58 and 0.98 eV at low frequency peak and high frequency peak, respectively. The lower frequency peak is attributed to the relaxation of the space charges associated with the oxygen vacancies at the grain boundary, whereas the higher frequency peak is due to oxygen vacancies relaxation inside the grains [31]. The relaxation process is considered to be the presence of short-range motion of charge carrier [32] and may be due to defects [30] at higher temperature. Figure 10 shows Arrhenius dependence for the relaxation time for (1 − x)BT–x BYYb (x = 0.02; 0.04; 0.06; 0.08; 0.11) at low frequency peak. The relaxation activation energies are about 1.2–2.2 eV. It is reported [33] that the activation energies of the hopping frequencies of the carriers is about 1.7–2.1 eV
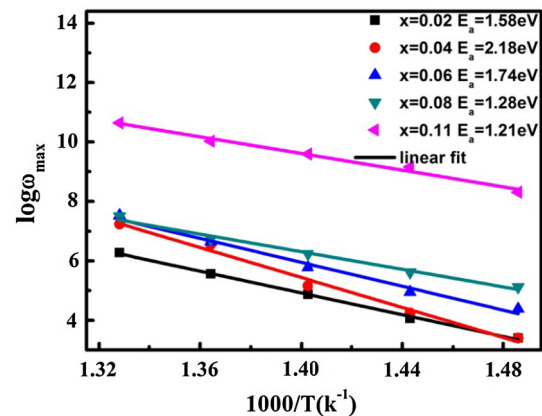
for $(Pb_{0.88}Sm_{0.08})$ $(Ti_{1-x}Mn_x)O_3$ ceramics above $T_m$ at low frequencies. The hopping processes could be associated with relaxations involving thermal motions of titanium ions $(Ti^{4+})$ [33]. Thus The relaxation process may not only be associated with oxygen vacancies relaxation but also related to thermal motions of titanium ions $(Ti^{4+})$ according to the relaxation activation energy value.

To analyze the microstructure of BT–BYYb, the complex impedance plate plots of (1 − x)BT–xBYYb (x = 0.02; 0.04; 0.06; 0.08; 0.11) at 400 °C have been shown in Fig. 11a–e. In which the main electric components for every sample are clearly detected. The center of semi-circle lies off the real axis (Z′) indicative of the non-Debye type relaxation with a distribute process instead of a single one. From x = 0.02–0.04, the boundary between the grain semi-circle and grain boundary semi-circle is blurred gradually. Every plot is resolved into two overlapped semi-circle, the poor separation of this overlapped semi-circle is due to the blocker size, which is referred to the pores that exist at the grain boundary [34].

The grain resistance and the grain boundary resistance were obtained by fitting the proposed circle with the help of Z-view software, activation energies are calculated from the temperature dependence resistance of the composites as shown in the Fig. 12. It obeys the Arrhenius law as follows;

$$R = R_0 \exp\left(\frac{-E_a}{K_B T}\right) \qquad (3)$$

where $R_0$ is the pre-exponential factor. $E_a$ is the activation energy of the conduction. Values in the ranges 0.3–0.4 and 0.6–1.3 eV in the low temperature region 200–400 °C have been associated with singly and doubly ionized oxygen vacancies, respectively [33]. In the high temperature region, mixed conduction governed by both doubly ionized oxygen and lead vacancies for F and Mn co-doped PZT
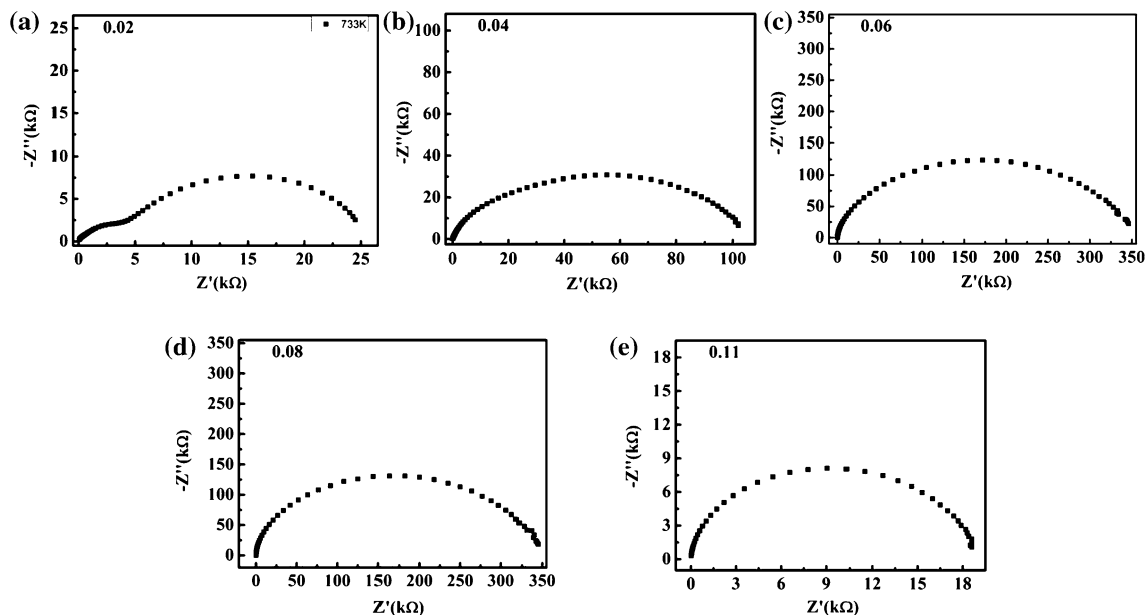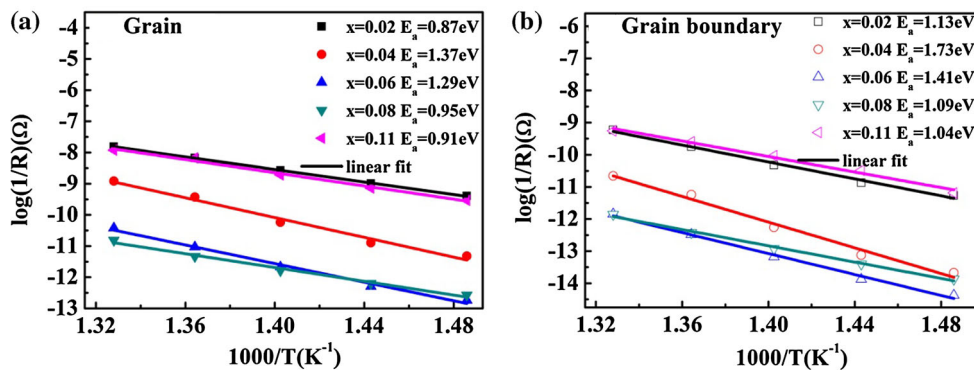
**Fig. 11** $(-Z'') - Z'$ plots for $(1 - x)BT–xBYYb$ (x = 0.02; 0.04; 0.06; 0.08; 0.11) at 400 °C

**Fig. 12** Arrhenus plot of grain and grain boundary with equivalent circuit at high temperatures ranges from 400 to 480 °C



[35] is responsible for the high activation energy of 1.47–2.02 eV. It is reported [33] that the activation energy in the $ABO_3$ perovskite structure decreases with increasing oxygen vacancy content. For the studied samples, The bulk activation energy decreases with the BYYb content for x > 0.02, which suggests an increase of oxygen vacancy concentration. Moreover, the value of the relaxation activation energy at 0.98BT–0.02BYYb is a little higher than that of bulk resistance, which is consistent with $(Pb_{0.88} Sm_{0.08}) (Ti_{1-x}Mn_x)O_3$ ceramics above $T_m$ [32] and indicates the different mechanism in the both process.

## 4 Conclusions

$(1 - x)BT–xBYYb$ (x = 0.01–0.12) ceramics were prepared by solid-state method. The crystal phase changes gradually from the tetragonal phase to the pseudocubic phase in the samples when 0.07 < x < 0.08. The average grain size decreases with x value. Dielectric properties are depressed and dielectric peaks are broadened with x. $T_m$ first increased and then decreased. BT–BYYb system exhibited diffused phase transition and good temperature stability. It can follow the modified the Curie–Weiss law and the transition diffuse $\gamma$ is 1 and 2, the different mechanism is responsible for in conduction and relaxation process.

## References

1. M.J. Pan, C.A. Randall, Electr. Insul. Mag. **26**, 44 (2010)
2. B. Tang, S.R. Zhang, X.H. Zhou, Y. Yuan, J. Mater. Sci. Mater. Electron. **18**, 541 (2006)

3. Y.C. Wu, S.F. Wang, D.E. McCauley, M.S.H. Chu, H.Y. Lu, J. Am. Ceram. Soc. **90**, 2926 (2007)
4. P. Gao, Y.P. Pu, P. Li, T. Wu, J. Mater. Sci. Mater. Electron. **24**, 3958 (2013)
5. L.X. Li, Y.R. Liu, M.J. Wang, N. Zhang, J.X. Chen, J. Mater. Sci. Mater. Electron. **25**, 4252 (2014)
6. S. Wang, H. He, H. Su, J. Mater. Sci. Mater. Electron. **24**, 2385 (2013)
7. L.X. Li, J.X. Chen, N. Zhang, Y.R. Liu, J.Y. Yu, J. Mater. Sci. Mater. Electron. **26**, 84 (2015)
8. G.F. Yao, X.H. Wang, Y.C. Zhang, Z.B. Shen, L.T. Li, J. Am. Ceram. Soc. **95**, 3525 (2012)
9. S.F. Wang, J.H. Li, Y.F. Hsu, Y.C. Wu, Y.C. Lai, M.H. Chen, J. Eur. Ceram. Soc. **33**, 1793 (2013)
10. S.S.N. Bharadwaja, J.R. Kim, H. Ogihara, L.E. Cross, S. Trolier-McKinstry, C.A. Randall, Phys. Rev. B **83**, 0241061 (2011)
11. H.Y. Guo, C. Lei, Z.G. Ye, Appl. Phys. Lett. **92**, 172901 (2008)
12. H. Ogihara, C.A. Randall, S. Trolier-McKinstry, J. Am. Ceram. Soc. **92**, 110 (2009)
13. T. Strathdee, L. Luisman, A. Feteira, K. Reichmann, J. Am. Ceram. Soc. **94**, 2292 (2011)
14. B. Xiong, H. Hao, S.J. Zhang, H.X. Liu, M.H. Cao, J. Am. Ceram. Soc. **10**, 3412 (2011)
15. J. Wang, Y. Liu, Q. Li, K. Lau, R.L. Withers, Z.R. Li, Z. Xu, Appl. Phys. Lett. **103**, 042910 (2013)
16. T.H. Wang, C.S. Tu, Y. Ding, T.C. Lin, C.S. Ku, W.C. Yang, H.H. Yu, K.T. Wu et al., Curr. Appl. Phys. **11**, 240 (2011)
17. M. Mahesh Kumar, A. Srinivas, S.V. Suryanarayana, J. Appl. Phys. **87**, 855 (2000)
18. S.O. Leontsev, R.E. Eitel, J. Am. Ceram. Soc. **92**, 2957 (2009)
19. H.C. Yu, Z.G. Ye, J. Appl. Phys. **103**, 034114 (2008)
20. S.Y. Zheng, E. Odendo, L.J. Liu, D.P. Shi, Y.M. Huang, L.L. Fan, J. Chen, L. Fang et al., J. Appl. Phys. **113**, 094102 (2013)
21. N. Raengthon, D.P. Cann, J. Am. Ceram. Soc. **95**, 1604 (2012)
22. N. Triamnak, R. Yimnirun, J. Pokorny, D.P. Cann, J. Am. Ceram. Soc. **96**, 3176 (2013)
23. I. Fujii, K. Nakashima, N. Kumada, S. Wada, J. Ceram. Soc. Jpn. **120**, 30 (2012)
24. X.C. Huang, H. Hao, S.J. Zhang, H.X. Liu, W.Q. Zhang, Q. Xu, M.H. Cao, J. Am. Ceram. Soc. **97**, 1797 (2014)
25. D.Y. Lu, M. Toda, J. Am. Ceram. Soc. **89**, 3112 (2006)
26. S.K. Jo, J.S. Park, Y.H. Han, J. Alloy Compd. **501**, 259 (2010)
27. K. Uchino, S. Nomura, Ferroelectrics **44**, 55 (1982)
28. Y.M. Li, W. Chen, J. Zhou, Q. Xu, X.Y. Gu, R.H. Liao, Phys. B **365**, 76 (2005)
29. K.C.V. Rajulu, B. Tilak, K.S. Rao, Appl. Phys. A **106**, 533 (2012)
30. R. Eewej, A. Oueslati, F. Hlel, J. Adv. Dielectr. **2**, 1230014 (2012)
31. A. Kaushal, S.M. Olhero, B. Singh, D.P. Fagg, I. Bdikin, J.M.F. Ferreira, Ceram. Int. **40**, 10593 (2014)
32. B.C. Sutar, R.N.P. Choudhary, P.R. Das, Ceram. Int. **40**, 7791 (2014)
33. A. Peláiz-Barranco, Y. González Abreu, R. López-Noda, J. Phys. Condens. Matter **20**, 505208 (2008)
34. B. Parija, S. Panigrahi, Ferroelectr. Lett. **39**, 38 (2012)
35. B. Guiffard, E. Boucher, L. Eyraud, L. Lebrun, D. Guyomar, J. Eur. Ceram. Soc. **25**, 2487 (2005)